EXPERIMENTAL TESTING OF NON-DUCTILE RC WALL BOUNDARY ELEMENTS

Scott J. Menegon, John L. Wilson, Nelson T. K. Lam and Emad F. Gad

Biography: Scott Menegon is a Research Fellow at Swinburne University of Technology and Senior Structural Engineer at Wallbridge Gilbert Aztec, Melbourne, Australia. He received his BEng (Hons) from Queensland University of Technology; MEngStruct from the University of Melbourne; and PhD from Swinburne University of Technology. His research interests include the design and experimental assessment of RC walls and the collapse behaviour of non-ductile RC buildings in lower seismic regions.

John Wilson is a Professor, Deputy Vice-Chancellor and Chief Executive Officer of Swinburne Sarawak, Malaysia. He received his BEng (Hons) from Monash University; MSc from the University of California, Berkeley; and PhD from the University of Melbourne. He is a member of ACI Committee 307 (Concrete Chimneys). His research interests are focused on earthquake engineering with a particular emphasis on the seismic performance of non-ductile RC columns and walls.

Nelson Lam is a Professor of Civil Engineering at the University of Melbourne, Australia. He received his BSc from the University of Leeds; MSc from Imperial College of Science & Technology; and PhD from the University of Melbourne. His research interests include the behaviour of RC buildings in lower seismic regions, ground motion analysis, structural dynamics and impact dynamics.

Emad Gad is a Professor and Dean of School of Engineering at Swinburne University of Technology, Melbourne, Australia. He received his BEng (Hons) from Monash University; and PhD from the University of Melbourne. His research interests include structural dynamics, light-framed steel construction and connections.

ABSTRACT

This paper presents an overview and results of a recent experimental testing program of non-ductile reinforced concrete (RC) wall boundary elements. The experimental program consisted of seventeen boundary element prism specimens that are meant to represent the end regions of non-ductile RC walls. The failure mechanisms of interest were global out-of-plane buckling and local bar buckling of the vertical reinforcement. The matrix of test specimens included: high and low slenderness ratios (i.e. high-to-thickness ratio); cast in-situ and precast wall construction methods; and specimens that were detailed with either a single central layer of vertical reinforcement or two layers of vertical reinforcement, one per face. Strain-rate affects were also assessed in the experimental program. The paper is concluded with a detailed discussion of the test results, comparisons with similar experimental programs and design models in literature and guidance on tensile strain limits for the displacement-based design of non-ductile RC walls.

Keywords: RC walls; RC wall prism testing; Non-ductile walls.

INTRODUCTION

The traditional failure mechanisms of RC walls that are observed under monotonic push-over loading are flexural failure (typically in the form of crushing of the compression concrete or fracturing of the tensile reinforcement), shear failure, or a combination of both. However, under cyclic response that typically occurs during earthquake ground excitations, additional failure mechanisms in RC walls can be developed, which would otherwise not be seem in monotonic response. This includes local buckling of the vertical reinforcement or out-of-plane instabilities that result in global out-of-plane buckling or premature concrete crushing failures.

An RC wall develops tension forces at one end of the wall and compression forces at the other end when in-plane lateral load is applied. Under large lateral loads the vertical reinforcement in the end region of the wall yields and develops plastic tension strains to resist the applied moment. When the lateral load decreases back to zero, the vertical reinforcement in the end region of the wall can still have significant residual plastic tension strains, resulting in horizontal cracks across the wall in this region not 'closing'. When the lateral load is reversed, the end region which was just in tension, is now in compression and the residual plastic tensile strains need to be eliminated via compression before these cracks can close and the end region of the wall can regain its axial stiffness. At this point, the vertical bar buckling or out-of-plane instability failure modes can be developed.

Out-of-plane instability failures were commonly observed following the recent 2010 Chile and 2011 Christchurch Earthquakes [1-3]. Since these two earthquakes, many research efforts have been initiated, including two separate large scale testing programs by Dashti, Dhakal and Pampanin [4, 5] and Rosso, Almeida and Beyer [6]. It should be noted though, that there is some dispute as to whether these observed failures we due to a 'global' out-of-plane buckling mechanism like what was report by Paulay and Priestley [7] some 25 years ago, or rather from

a ‘localised’ out-of-plane instability caused by asymmetric crushing/spalling of concrete and buckling of the vertical reinforcement (refer Segura and Wallace [8]).

The experimental program in this study focused on walls with non-ductile detailing. Non-ductile detailing would include walls classified as ‘ordinary’ to the American Concrete Code (i.e. ACI 318 [9]), ‘non-ductile’ to the New Zealand Concrete Standard (i.e. NZS 3101 [10]) or ‘limited ductile’ to the Australian Concrete Standard (i.e. AS 3600 [11]). Non-ductile boundary element detailing often consists of providing lapped ‘U’ bars at the ends of walls that are lapped with the horizontal reinforcement and enclosure the vertical reinforcement. The spacing of these of ‘U’ bars are relatively wide, often greater than the thickness of the wall. In some instances, non-ductile walls are also detailed without these ‘U’ bars, meaning the vertical bars in the end region of the wall are not enclosed by horizontal bars or ties.

This is in contrast to walls that are detailed for ductility (i.e. ‘special structural walls’ to ACI 318), where the end regions of the walls require ‘special boundary elements’ that have closed ligatures and/or cross ties that enclose the vertical bars and confine the compression region of the wall. ACI 318 allows the designer to assess the need for special boundary elements by either adopting a displacement-based approach where the detailing requirements are based on the expected lateral displacement of the wall or using a conservative stress-based approach that is similar to the requirements of the 1995 version of ACI 318. Similarly, AS 3600 adopts this conservative stress-based approach for determining boundary element requirements in walls that are detailed for ductility. However, a displacement-based approach is not provided in AS 3600.

RESEARCH SIGNIFICANCE

RC walls are a very common and widely used lateral load resisting system for multi-storey buildings in many parts of the world. Non-ductile RC walls are commonly found in many older existing buildings in higher seismic regions and widely used as the standard form of

construction in regions of lower seismicity [12]. This experimental program explicitly considers non-ductile wall detailing and proposes new tensile strain limits for displacement-based or general non-linear assessment methods to prevent premature buckling failure. The experimental program provides valuable insights, which will inform better detailing practices that will improve the overall performance of such walls.

EXPERIMENTAL INVESTIGATION

Testing Methodology and Background

The experimental testing program consisted of various boundary element test specimens of different dimensions and reinforcement configurations. The specimens represented the end region of a non-ductile RC wall or building core, which under cyclic lateral loads, is essentially subjected to cyclic tension-compression axial load, as illustrated in **Fig. 1**. As such, the individual test specimens are subjected to cyclic axial tension-compression loading to simulate the system level behaviour shown in **Fig. 1**. This has become a popular form of experimental testing in recent years (e.g. [13-18]) and is commonly referred to as 'prism testing'.

This form of testing allows for the performance of various RC wall end region detailing techniques to be experimentally assessed for different failure mechanisms (e.g. localised vertical bar buckling or global out-of-plane instability failure mechanisms discussed previously) without having to perform costly full-scale in-plane RC wall tests. Vertical bar buckling in non-ductile walls is prevented by the cover concrete staying intact and providing lateral restraint. This mechanism that prevents bar buckling is difficult to assess theoretically and much easier to assess experimentally. This is in contrast to ductile end regions, which have tightly spaced transverse reinforcement that provides additional restraint against vertical bar buckling.

The prism testing performed in literature currently includes: 9 specimens tested by Patel et al. [13], which were small specimens with one central bar; 1 specimen tested by Segura et al. [14],

which was a ductile prism specimen with a small height-to-thickness ratio of 6.0; 16 specimens tested by Taleb et al. [15], which were all ductile prism specimens with small to moderate height-to-thickness ratios of 5.4 to 8.8; 33 specimens tested by Welt et al. [16], which included both non-ductile and ductile prism specimens with small to moderate height-to-thickness ratios of 4.0 to 8.9, however only 1 non-ductile specimen was tested under cyclic actions with the others under monotonic loading; 8 specimens test by Hilson [17], which were all non-ductile prism specimens with a small height-to-thickness ratio of 5.0; and 12 specimens tested by Rosso et al. [18], which were non-ductile specimens with central reinforcement and very slender height-to-thickness ratios of 24 to 30. The studies by Hilson [17] and Rosso et al. [18] represent the best test programs identified in literature for non-ductile boundary elements. The test specimens in this study have different reinforcement configurations and height-to-thickness ratios than the specimens in [17, 18], in addition to also including specimens that are constructed with lap splices of the vertical reinforcement and using precast grout tube connections, both of which are commonly detailing aspects of non-ductile walls.

Test specimen overview

The experimental testing program consisted of seventeen prism specimens. A summary of all the prism specimens is provided in **Table 1** and the reinforcement detailing for each specimen is presented in **Fig. 2**.

The first six specimens (i.e. P01 to P06) were ‘type 1’ specimens, which were higher slenderness ratio (i.e. height-to-thickness ratio) boundary elements and 2000 mm tall, 450 mm long and 130 mm thick. The other eleven specimens (i.e. P07 to P17) were ‘type 2’ specimens, which were lower slenderness ratio boundary elements and 800 to 850 mm tall, 450 mm long and 130 to 150 mm thick. The failure mechanisms of interest for the type 1 and type 2 specimens was primarily global out-of-plane buckling and local bar buckling respectively (refer **Fig. 1**). Different reinforcement ratios and configurations were considered for both types of specimens. The type 1 specimens had vertical reinforcement ratios varying from 0.6% to 2.1% and

similarly, the type 2 specimens had vertical reinforcement ratios varying from 0.4% to 2.1%. Both types had specimens with reinforcement 'each face' (i.e. vertical and horizontal bars on each face of the specimen) and 'central' (i.e. one layer of vertical and horizontal bars located centrally in the specimen).

The specimens were constructed using D500N or D500L reinforcement in accordance with AS/NZS 4671 [19]. D500N and D500L denotes normal and low ductility reinforcement respectively, with a minimal characteristic yield stress 500 MPa. The minimum characteristic strain hardening ratios are 1.08 and 1.03 and the minimum characteristic uniform elongations are 5% and 1.5% respectively. N12 denotes a 12 mm nominal diameter reinforcing bar that is grade D500N. Similarly, L11.9 denotes a 11.9 mm nominal diameter reinforcing bar that is grade D500L.

The specimens were constructed using a standard N40 grade concrete mix with a minimum characteristic 28-day cylinder compressive strength of 40 MPa and a maximum aggregate size of 14 mm. The compressive strength of the concrete was determined on test day for each specimen using 100 mm diameter and 200 mm long cylinder tests. The concrete strength on test day varied from 33.0 to 56.2 MPa. Further details regarding the material properties for the concrete and reinforcement (including reinforcement stress-strain curves) used in the test specimens are presented in [20].

Specimens P07 to P10 were constructed with a crack propagator at mid-height (as shown in **Fig. 2**) to ensure a crack was initiated at this exact location where strain gauges were attached on the vertical bars.

Specimens P11 to P17 were constructed with splices of the vertical bars at the base of the specimen, since non-ductile reinforcement detailing in lower seismic regions (e.g. Australia) typically allows lap splices to be included in the plastic hinge region of the wall. Specimens P11 to P14 had traditional lap splices. The lap splice length (as shown in **Fig. 2**) was calculated

in accordance with the Australian Concrete Standard AS 3600 [11], which is a function of: the yield stress of the bar; the characteristic compressive strength of the concrete; the bar diameter; and either the clear cover or the vertical bar spacing.

Specimens P15 to P17 had grout tube connections (refer **Fig. 2**), which are industry standard precast connections for walls panels in multi-storey construction in both Australia [12] and New Zealand [21]. The grout tube connection has a corrugated grout tube sleeve cast vertically into the base of the panel that slots over a dowel bar cast into the supporting structure below the panel. The grout tube is typically at least twice the diameter of the dowel bar, allowing for a generous amount of construction tolerance so the panels can be easily erected and accurately aligned on site. After the panels are erected on site, the base of the panel is 'dry packed' with a cementitious grout. The grout tube is usually then filled the next day using a flowable high strength cementitious grout.

The grout tube embedment length for P15 to P17 (as shown in **Fig. 2**) was specified to match typical values adopted in industry. There is no 'codified' approach in AS 3600 or 'industry standard' for calculating grout tube embedment lengths in Australia.

Designers often justify a smaller lap length than the equivalent lap splice in a cast in-situ member by assuming the high-strength grout that surrounds the dowel bar is confined by the corrugated grout tube itself. This confinement then allows the yield stress of the dowel bar to be transferred to the high-strength structural grout over a reduced development length. Subsequently, because the corrugated grout tube has a significantly increased diameter compared to the dowel bar, the equivalent yield stress of the dowel bar can then be transferred to the concrete member over the same reduced development length. The authors do not necessarily endorse this approach and suggest further investigation of this bond stress transfer mechanism is required.

Further test specimen details and construction drawings for each specimen are provided in [20].

Test Setup and Instrumentation

The specimens were tested in the Smart Structures Laboratory (SSL) at Swinburne University of Technology. All seventeen test specimens were tested under cyclic axial tension-compression loading in the MTS 1MN uniaxial test machine, except P01 and P05, which were tested under monotonic compression loading in the Instron 5MN uniaxial test machine.

Test specimens P11 to P17 were tested with an out-of-plane horizontal roller support at mid-height to prevent any possible out-of-plane instability failure mechanisms developing, since the primary failure mechanism of interest for the type 2 specimens was local bar buckling of the vertical reinforcement. Despite this, specimens P07 to P10 were not tested with the mid-height out-of-plane roller support.

A combination of physical instrumentation attached to the tests specimens and a contactless photogrammetry system was used to monitor and measure the behaviour and response of the test specimens. Post yield strain gauges were attached to the vertical reinforcement on specimens P07 to P10. The gauges were located at mid-height of the specimens in line with the crack propagator (refer **Fig. 2**).

Loading Protocol

Two different primary types of loading protocols were adopted for testing the boundary element test specimens. The first type of loading protocol was a quasi-static monotonically increasing axial compression load, which was performed in the 5 MN Instron test machine. The second type of loading protocol was cyclic axial tension-compression loading, which was performed in the 1 MN MTS test machine. Further, the cyclic axial tension-compression loading was applied as a quasi-static loading protocol for all the specimens, except P04, where it was applied as a quasi-dynamic loading protocol. The latter was used to assess whether loading strain rate affects the out-of-plane buckling behaviour of RC walls. The loading protocols used for the seventeen boundary element test specimens is summarised in **Table 2**.

Test specimens P01 and P05 had a quasi-static monotonic axial compression loading protocol. The specimens were in axial compression under a displacement-controlled protocol until failure.

Test specimens P02, P03, P06 to P17 had a quasi-static cyclic axial tension-compression loading protocol. Each respective specimen was subjected to a preselected tension displacement increment in displacement-controlled behaviour. The load was then reversed and axial compression was applied to the specimen until the cracks closed (i.e. axial stiffness was regained) or the capacity of the machine was reached (i.e. 1 MN). If the specimen was able to recover its axial stiffness, i.e. the cracks closed without any localised damage occurring, the specimen was then subjected to a larger tension displacement and the process repeated.

The failure mechanisms of interest in this testing, i.e. global out-of-plane buckling and local bar buckling, occur after the element is subjected to reversed axial compression prior to the cracks closing. If the cracks close without any localised damage occurring, the wall can regain its axial stiffness and these failure mechanisms are not able to occur.

The specimens were typically loaded to tension displacement increments that approximately equalled 1%, 2%, 3%, 4% and 5% average strain across the height of the specimen (e.g. 1% average strain in P01 equals $2000 \times 0.01 = 20\text{mm}$), unless failure occurred prior. Additionally, test specimens P07 to P17 were initially loaded to a tension force that equalled an elastic stress between 350 to 450 MPa (i.e. 70% to 90% of the characteristic yield stress) being reached in the vertical reinforcement, before starting the larger inelastic tension displacement increments above.

Test specimen P04 was tested using a quasi-dynamic cyclic axial tension-compression loading protocol. The loading protocol was much the same as the quasi-static loading protocol described above, however the loading rate was significantly faster and intended to represent indicative strain rates that would be typical of the response seen during an earthquake.

The specimen was initially loaded at a velocity of 140 mm/s (i.e. a strain rate of 7% per second), however the test machine was unable to apply the loading at this rate, as shown by the commanded and actual displacement signals in **Fig. 3**. Therefore, the test was paused at approximately the 2 second mark and the loading rate was adjusted to 100 mm/s (i.e. a strain rate of 5% per second). The test machine however, was still unable to achieve the slower loading rate of 100 mm/s and the actual loading rate for the third and fourth loading cycles was approximately 50 and 70 mm/s respectively (i.e. a strain rate of 2.5% and 3.5% per second respectively). Strain rates of 2.5% to 3.5% per second would still be considered representative of the response expected during an earthquake [22, 23].

EXPERIMENTAL RESULTS AND DISCUSSION

Type 1 specimens – P01 to P06 – high slenderness ratio

Quasi-Static Monotonic Axial Compression Tests – Specimens P01 and P05

Test specimens P01 and P05 failed in combined compression and eccentric bending, which resulting in a diagonal shear failure developing at the base of the wall, across the thickness of the wall, as shown in **Fig. 4(a)** and **Fig. 4(e)** respectively. Despite best efforts to locate the specimen in the centre of the machine and apply concentric loading, it is believed the walls were loaded with a slight horizontal eccentricity, resulting in the combined compression and bending behaviour.

Specimens P01 and P05 failed at a total vertical load of 2040 and 1954 kN respectively. The failure loads corresponded to 78% and 62% respectively of the theoretical maximum capacity of the concrete ignoring slenderness effects (i.e. the gross cross-sectional area multiplied by the concrete cylinder strength on test day). The average strain, taken across the full height of the specimen, at failure was 0.18% and 0.15% respectively. The force-displacement response of both specimens is presented in **Fig. 5** (the normalised force is equal to the applied force divided

by the concrete cylinder strength on test day times the gross cross-sectional area and the average strain is equal to the overall displacement divided by the specimen height).

Specimen P01 had two layers of vertical reinforcement, i.e. 3-N12 on each face, which would have resulted in the minor axis bending moment capacity of the wall being significantly higher than specimen P05, which only had 3-N12 bars placed centrally. This increased minor axis bending capacity in P01 seemed to allow the specimen to overcome more of the slenderness effects and allow a higher normalised force to develop (refer **Fig. 5**).

The ultimate compression capacity of each wall was calculated using the simplified design formulas proposed by both ACI 318 [9] and AS 3600 [11], i.e. **Eq. 1** and **2** respectively. It should be noted some of notation in **Eq. 1** and **2** has been adjusted for consistency.

$$P_u = 0.55 f_c' L_w t_w \left[1 - \left(\frac{kH}{32 t_w}\right)^2\right] \quad (1)$$

$$P_u = 0.6 f_c' L_w (t_w - 1.2e - 2e_a) \quad (2)$$

Where: f_c' is the concrete characteristic compressive strength; L_w is the length of the wall; t_w is the thickness of the wall; e is the load eccentricity, taken as $0.05 t_w$ for walls with a continuous cast in-situ slab over; e_a is an additional eccentricity taken as $(kH)^2/(2500 t_w)$; H is the height of the wall between stories; and k equals 0.8 and 0.75 for **Eq. 1** and **2** respectively if restraint against rotation is provided at both ends, otherwise it is taken as 1.0.

The ACI 318 formula (i.e. **Eq. 1**) resulted in an ultimate compression capacity of 1225 and 1467 kN respectively for specimens P01 and P05, which means the specimens were able to withstand 1.66 and 1.33 times the theoretical ultimate compression capacity, respectively. Similarly, the AS 3600 formula (i.e. **Eq. 2**) resulted in an ultimate compression capacity of 1308 and 1565 kN respectively for specimens P01 and P05, which means the specimens were able to withstand 1.56 and 1.25 times the theoretical ultimate compression capacity, respectively. These results suggest the ACI 318 and AS 3600 formulas for simplified wall

design are appropriate for lightly reinforced walls with a central layer of vertical bars, yet simultaneously, also somewhat conservative for walls with two layers of vertical reinforcement.

Quasi-Static Cyclic Axial Tension-Compression Tests – Specimens P02, P03 and P06

Test specimens P02 and P03 failed in the desired out-of-plane buckling failure mechanism, as shown in **Fig. 4(b)** and **Fig. 4(c)** respectively. The specimens were able to undergo 2.0% and 1.8% average tension strain respectively, without an out-of-plane buckling failure occurring in the subsequent reversed axial compression load cycle. When the specimens were then subjected to larger average tension strains of 3.0% and 2.8% respectively, out-of-plane buckling occurred in the subsequent reversed axial compression load cycle. This out-of-plane buckling mechanism then results in axial load failure of the boundary element, occurred at a load equal to about 10% of the gross compression capacity of the specimen.

The force-displacement and out-of-plane buckling behaviour of specimens P02 and P03 are presented in **Fig. 6** and **Fig. 7** respectively (negative values correspond to axial tension and positive values correspond to axial compression). The normalised force in these figures is equal to the force divided by the gross cross-sectional area of wall multiplied by the concrete cylinder strength for the respective specimen. The average tension strain is equal to the tension displacement divided by the height of the wall, i.e. 40 mm displacement equals 2% average tension strain ($40/2000 = 0.02$).

The observed out-of-plane buckling behaviour is summarised as follows:

1. The RC element is subjected to an axial tension displacement that cracks the concrete and forces the tension load to be transferred to the vertical reinforcement. The reinforcement then yields and resists the axial tension displacement through a combination of elastic elongation and inelastic plastic elongation.
2. The tension load on the RC element is released and the in-plane displacement is reduced by the elastic portion of elongation in the reinforcement being recovered. At this point there

are residual cracks ‘still open’ due to the inelastic plastic strains in the reinforcement from the previous tension displacement load cycle.

3. The RC element is subjected to compression. The compression load allows the inelastic plastic strains to be recovered and initiates closing of the residual crack width. As the residual cracks begin to close, out-of-plane displacement of the wall initiates and progressively increases as the cracks start to close.
4. A bifurcation effect occurs, where depending on the amount of inelastic plastic tension strain in the reinforcement and the overall slenderness ratio of the wall, either:
    i. The wall ‘self-corrects’ and the out-of-plane displacement reduces back to zero as the cracks begin to close and the axial stiffness of the wall is regained; or
    ii. The wall cannot self-correct, the axial stiffness of the wall cannot be regained and out-of-plane buckling failure occurs.

Photo series illustrating both the initiation of buckling followed by the self-correcting behaviour (i.e. steps 1–4i) are show in **Fig. 8(a)** to **8(d)** and the initiation of buckling followed by global out-of-plane buckling failure (i.e. steps 1–4ii) are presented in Menegon [20].

Test specimen P06, unlike specimen P02 and P03, failed due to local bar buckling of the vertical reinforcement, prior to an out-of-plane buckling failure being able to develop. Specimen P06 behaved similar to specimens P02 and P03 during the first loading cycle (as shown in **Fig. 6** and **Fig. 7**). However, during load cycle two, after the load reversal from axial tension to axial compression and the wall regained its initial axial stiffness, local bar buckling of the vertical reinforcement occurred. Specimen P02 also had significantly higher amounts of out-of-plane displacement for the relative equivalent tension strain in the previous reversed load cycle compared to P02 and P03 (as shown **Fig. 7**) due to having just a single central layer of vertical reinforcement. The behaviour of specimen P06 during load cycle two, up to failure, is shown in **Fig. 8**.

It should be noted that the initial loading cycle for specimen P06 was interrupted due to a system error in the test machine. This did not affect the behaviour/response of the specimen, however it did result in the first portion of test data not being captured, as indicated by the dashed line in **Fig. 6**.

The behaviour of specimen P06 was attributed to the irregular and sparse distribution of cracking, which was due to the low percentage of vertical reinforcement. This resulted in the formation of a large major crack just below the mid-height of the wall (refer **Fig. 8(a)**). During load cycle 2, the maximum axial tension displacement was 40 mm and this major crack had a crack width of approximately 12 mm, meaning 30% of the axial tension displacement was concentrated at one location. The large concentration of displacement across this single crack would have corresponded to a very large local tensile strain in the reinforcement at this location. This localised tensile strain concentrated due to the lack of distributed cracking (unlike the well distributed closely spaced cracking that was observed in specimens P02 and P03) initiated the local bar buckling behaviour of the vertical reinforcement in P06.

Quasi-Dynamic Axial Tension-Compression Tests – Specimen P04

The results of the quasi-dynamic axial tension-compression test specimen (i.e. P04), which was a replica of specimen P03, are shown previously in **Fig. 6** and **Fig. 7**. The force-displacement and out-of-plane buckling behaviour of P04 is overlaid on P03 in these figures and show the response is very similar. This indicates that strain rate has little effect on the out-of-plane buckling behaviour.

Type 2 specimens – P07 to P17 – low slenderness ratio

A variety of different failure modes were observed in specimens P07 to P17. These included: local bar buckling; out-of-plane instabilities; bar fracturing; and debonding of the vertical lap splice at the base of the specimen. Failure photos of P07 to P10 are shown in **Fig. 9** and force-displacement response of P07 to P11, P13 and P15 to P17 are shown in **Fig. 10** (negative values correspond to axial tension and positive values correspond to axial compression). The response

is presented in terms of the normalised force and average global strain. The former is equal to the force divided by the tensile yield capacity of the specimen (i.e. the yield capacity of the vertical reinforcement) and the latter is equal to the axial displacement divided by the height of the specimen. For test specimens P15, P16 and P17 where the cross-sectional area of vertical reinforcement and dowel bars was not equal, the normalised force is presented with respective to the lesser of the two. This means the normalised force for test specimen P15 is with respect to the tensile yield capacity of the dowel bars and for test specimens P16 and P17 it is with respect to the tensile yield capacity of the vertical reinforcement.

The results of P12 and P14 are not presented in **Fig. 10**. Specimens P12 and P14 prematurely failed due to bond failure of the lap splice (i.e. unzipping). The failure of these specimens was due to construction problems with the specimens and not reflective of the specimen detailing.

Vertical bar buckling failures – Specimens P07, P10, P11 and P13

The vertical bar buckling failures of P07 and P10 are shown in **Fig. 9(a)** and **Fig. 9(d)** respectively. Bar buckling occurred in specimen P07 in the reversed axial compression cyclic after being subjected to a 40 mm axial tension displacement, which corresponds to an average tension strain of 5%. The strain gauges on the vertical bars 'saturated' after the previous cycle, so the local tension strain corresponding to the 5% average tension strain load increment was unknown. However, the previous load cycle (i.e. average tension strain of 4%) had a local tension strain of 6.2% in the reinforcement. Using this data and a tension stiffening modelled developed by the authors (refer Menegon [20]), the local tension strain corresponding to the loading cycle with an average tension strain of 5%, was calculated to be approximately 7.3%. This means that the vertical reinforcement could be subjected to a local tension strain of about 6–7% before local bar buckling was initiated.

Bar buckling occurred in specimen P10 in the reversed axial compression cycle after being subjected to a smaller axial tension displacement of 23 mm, which corresponded to an average tension strain of 2.8%. The local tension strain at this point was 4.5%. It is believed that vertical

splitting of the specimen, which can be seen **Fig. 9(d)**, resulted in vertical bar buckling being initiated at a lower tension strain than specimen P07. This indicates that local bar buckling is potentially worse in singularly reinforced walls, since in doubly reinforced walls there would normally be some nominal cross ties in non-ductile walls (e.g. 'U' bars are each end of the wall [12]), which would limit vertical splitting failures.

Bar buckling occurred in specimens P11 and P12 in the reversed axial compression cycles after being subjected to tension displacements of 31 and 33 mm, which corresponded to average tension strains of 3.8% an 3.9% respectively. The corresponding local tension strains in the reinforcement in these specimens was calculated to be approximately between 6 and 7%, which is in good agreement with P07.

Out-of-plane buckling failures – Specimen P08

Specimen P08 failed via global out-of-plane buckling, as shown in **Fig. 9(b)**. The out-of-plane buckling mechanism matched what was observed in specimens P02, P03 and P04. The global buckling occurred after a tension displacement of 37 mm was applied, which corresponded to an average tension strain of 4.7% and a local strain in the reinforcement of 4.8%. The results of P08, similar to P07, suggest that the vertical reinforcement in non-ductile RC walls can be subjected to a local tension strains of 5% without local bar buckling occurring in subsequent reversed load cycles.

Vertical bar fracturing failures – Specimens P09, P15, P16 and P17

Specimen P09 failed via fracturing of the vertical reinforcement. The low percentage of vertical reinforcement in P09 allowed for minimal cracking to be developed (i.e. cracks only developed at the top and bottom and at mid-height), which resulted in large concentrations of plastic strain (refer **Fig. 9(c)**).

Specimens P15, P16 and P17, which were constructed using precast connections (i.e. grout tube) at the bottom of the specimens, also failed via fracturing of the vertical reinforcement. P15 was detailed such that the dowel connection was the 'weak' point. This was done by using

3-N16 dowel bars and then 8-N12 vertical bars in the wall section above, meaning the vertical reinforcement in the wall above had 1.5 times the capacity of the dowel bars in tensions. As a result, the majority of the displacement was concentrated at the base and only hairline cracks developed across the height of the specimen. The wall was able to be subjected to a force corresponding to an average tension stress of 673 MPa in the vertical bars before bar fracture occurred, which was 3% less than the actual ultimate stress of the individual bars. This indicates that the tension load was not evenly distributed amongst the three dowel bars, albeit, only by a minor amount. The grout tubes prevented any local buckling of the dowel bar from occurring.

Specimen P15 was able to resist 406 kN in tension prior to the first bar fracture occurring. This means that the 40 mm diameter corrugated grout tubes, which were 500 mm long, were able to develop, at a minimum, an average bond stress of 2.2 MPa. This corresponds to a bond stress of approximately $0.4\sqrt{f_{cm}}$, where f_{cm} is the average concrete cylinder compressive strength. The maximum bond stress of the corrugated grout tubes would likely be significantly higher than this, however this does provide a good indication of the minimum average bond stress of the grout tubes.

Specimen P16 was detailed such that the section of wall above the dowel connection was the 'weak' point. This was done using 4-N20 dowel bars and 6-N12 vertical bars in the wall section above, meaning the dowel bars had 1.9 times the capacity of the vertical bars in the wall section. As a result, the majority of the displacement was concentrated in the 350 mm section of wall above the grout tube connection and only hairline cracks developed across the grout tube region of the specimen.

The inelastic tension displacement in P16 was concentrated across three major cracks. This meant the specimen failed at a much small tension displacement increment than P11 and P13. Interestingly enough, despite the development of a major crack, with what would have had a significantly high amounts of local tension strain in the reinforcement, unlike specimens P07,

P10, P11and P13, bar buckling was not initiated. Similar to P15, the wall was able to developed an average tension stress of 619 MPa, which was 5% less than the actual ultimate stress of the individual bars. Meaning the tension load was not evenly distributed amongst the six vertical bars.

It is difficult to ascertain from the results of P15 and P16 as to whether better performance will be achieved from a precast RC wall if it is designed to have the 'weak' point above the grout tube or at the base of the wall. If the latter occurs, the inelastic behaviour will be concentrated at the base of the wall and a 'singe-crack' mechanism will be formed. This type of mechanism in cast in-situ walls has been heavily researched, particularly following observations of damage in RC walls after the 2011 Christchurch earthquake, and found to result in quite poor seismic performance (e.g. [24-26]). However, in precast walls with a grout tube connection, it seems that the grout has poorer inelastic bond strength properties compared to in-situ concrete and as such, much greater yield penetration occurs prior to bar fracturing. This results in significantly more inelastic behaviour or a 'wider' crack at the base of the wall. Further, in large-scale precast building core testing performed by the authors (refer [20, 27]), the foundation block and grout tube prevent bar buckling of the dowel bar (similar to P15), allowing tensile fracturing of the dowel bar to be the ultimate failure mechanism. Alternatively, if the weak point is above the grout tube, a typical plastic hinge could be developed, which has traditionally been the desirable failure mechanism for walls. Further analytical studies are recommended in this instance before design advice is provided.

Specimen P17 was detailed to generally match P16, except the vertical bars were substituted for low ductility reinforcement (i.e. D500L to AS/NZS 4671 [19]), which is commonly used, yet ill-advised [28], in precast wall construction in Australia. Precast contractors prefer using low ductility reinforcement because it comes in sheets of welded mesh, which is easier to place and tie off. Low ductility reinforcement has a very small minimum characteristic strain

hardening ratio and typically, the little strain hardening it can sustain, occurs over very short region from the onset of yielding to about 1% strain being reached. Between 1% strain and the uniform elongation of the bar, typically only a minor amount of additional strain hardening occurs [28]. This extremely inhibits a member's ability to develop distributed cracking with distributed plasticity. This was observed experimentally in P17, where despite three main cracks developing between the top of the grout tube connection and the top of the specimen, once the vertical bars yielded, all the inelastic deformation was concentrated in a single crack, which resulted in bar fracture of the vertical reinforcement at a very small tension displacement.

COMPARISON TO PREVIOUS STUDIES

Out-of-plane buckling

Test results for specimens P02, P03 and P08, which failed due to out-of-plane buckling, were compared to the models proposed by Paulay and Priestley [7] and Chai and Elayer [29], which are presented in **Eq. 3** and **4** respectively, in **Fig. 11**.

$$\varepsilon_{sm} = 8\beta\left(\frac{t_w}{L_o}\right)^2 \xi_c \tag{3}$$

$$\varepsilon_{sm} = \frac{\pi^2}{2}\left(\frac{t_w}{L_o}\right)^2 \xi_c + 3\varepsilon_{sy} \tag{4}$$

Where: ε_{sm} is the maximum tensile strain before out-of-plane buckling occurs in the subsequent reversed load cycle; t_w is the thickness of the wall; L_o is the buckling length; β is the ratio of the distance to the outer layer of vertical reinforcement to the thickness of the wall, i.e. $\beta = d/t_w$; ξ_c is the critical normalized out-of-plane displacement, i.e. $\xi_c = 0.5\left(1 + 2.35m - \sqrt{5.53m^2 + 4.7m}\right)$; and m is the mechanical reinforcement ratio of the boundary element, i.e. $m = p_v f_{sy}/f_c'$.

While these proposed models are for calculating the maximum tensile strain in the reinforcement, the Chai and Elayer [29] model, which was developed using a comprehensive study consisting of 14 test specimens, was developed and calibrated using the average tension

strain values from the test specimens, not the actual local tension strain in the reinforcement itself at the location of the horizontal cracks. Further, Paulay and Priestley [7] also argue that when calculating the slenderness ratio, it should be the minimum of the plastic hinge length divided by the thickness of the wall or 80% of the clear storey height divided by the thickness of the wall. Therefore, the slenderness of P02 and P03 would be 12.3, i.e. $0.8 \times 2000/130 = 12.3$, and for P08 it would be 3.1, i.e. $0.8 \times 800/130 = 4.9$. However, given buckling is first initiated at mid-height of these specimens, the wall thickness of P08 should be reduced to 100 mm to account for the crack propagator, which means its slenderness would be 6.4.

It can be seen in **Fig. 11** that the Paulay and Priestley [7] model is quite conservative, whereas the Chai and Elayer [29] model seems to better predict maximum tensile strains prior to buckling occurring on subsequent reversed axial compression load cycles. Further, both models give maximum strains that correspond to the average tension strain of the section, not the local tensile strain in the reinforcement, since they were developed using average strains calculated across a gauge length rather than local reinforcement strains. The difference between these values can vary significantly and is largely dependent on crack spacing of the section. The authors have proposed a generalised tension stiffening model for determining the ratio between the two [20].

Hilson [17] performed a series of prism tests on eight specimens, which were meant to represent ordinary boundary elements to ACI 318 and had similar reinforcement detailing to the specimens in this experimental program. The specimens were 30 in. (765 mm) tall and had a thickness of 6 in. (152 mm). Four of these specimens failed in an out-of-plane buckling failure mode after being subjected to average tension strains of about 4.5%. This is also somewhat in agreement with the models proposed by Paulay and Priestley [7] and Chai and Elayer [29].

Local bar buckling

Test specimens P07, P11 and P13 showed that local tension strains of about 6–7% could be developed in the reinforcement before local buckling of the reinforcement was observed in the subsequent reversed load cycle. Where specifically, P07 was able to developed a local tension strain of 7.3% in the reinforcement, which corresponded to an average tension strain of 5% across the full height of the specimen, before local bar buckling was observed. In this instance, the difference between the local and average tension strains was approaching a factor of 1.5.

Three of the prism specimens tested by Hilson [17] failed due to local buckling of the vertical reinforcement. In this testing, bar buckling was observed in subsequent reversed load cycles after tension strains of 3–4.5% were applied to the specimens. The tensions reported in this work however, were average tension strains over a gauge length determined using LVDTs, as opposed to local strains in the reinforcement measured using post-yield strain gauges. Using the tension stiffening modelling developed by Menegon [20], it was calculated that these average tension strains correspond to local tension strains in the reinforcement of around 4.2–5.6%. These maximum local tension strain values in the reinforcement are still somewhat lower than the values observed in this experimental study.

PROPOSED DESIGN GUIDANCE FOR NON-DUCTILE WALLS

Seismic design in regions of lower seismicity, e.g. Australia, typically consists of checking a building for a no collapse performance objective under a rare (i.e. long return period) earthquake event. Buildings are rarely checked for service or operational performance objectives for short return period events because earthquakes are so uncommon in low seismicity intraplate regions. This means the sole performance objective of interest is usually to ensure that the building and its lateral load resisting elements can maintain axial load carry capacity following the earthquake event.

It is being recommended that a reinforcement local tensile strain limit of 4.0% for non-ductile walls is adopted for a no collapse performance objective to prevent local bar buckling of the

vertical reinforcement. This recommendation is based on both the results of this experimental study and experimental work performed by Hilson [17], which suggested local tension strains in the vertical reinforcement of about 6–7% and 4.2–5.6% respectively could be developed before being susceptible to bar buckling on reversed load cycles.

Additionally, the Chai and Elayer [29] (i.e. **Eq. 4**) model is recommended to be used on a case-by-case basis to determine a tensile strain limit to ensure out-of-plane buckling instabilities cannot be developed.

SUMMARY AND CONCLUSIONS

The key results from the boundary element prism testing are as follows:

1. The simplified design formulas in ACI 318 and AS 3600 for the compression capacity of an RC wall are appropriate for lightly reinforced walls with a central layer of vertical bars, yet simultaneously, also somewhat conservative for walls with two layers of vertical reinforcement.
2. Global out-of-plane buckling/instability can occur when an RC element is in compression and tries to overcome the residual plastic tension strains sustained in the previous reserved cyclic load case. The element undergoes a bifurcation effect where it either overcomes these residual plastic tensile strains or said failure mechanism ensues, resulting in axial load failure at a load equal to about 10% of the gross compression capacity.
3. Strain rate effects were shown to have no effect on the out-of-plane buckling mechanism of RC walls. This means traditional quasi-static loading protocols are appropriate for experimentally assessing this behaviour and type of failure mode for walls.
4. Bar buckling in limited ductile RC construction is a complex failure mechanism as it relies on the cover concrete to provide lateral restraint against buckling. The buckling force is dependent on both the residual amount of inelastic tension strain in the bar and the residual crack width. It is being recommended that a reinforcement tensile strain limit of 4.0% for

non-ductile walls is adopted for a no collapse performance objective to prevent local bar buckling of the vertical reinforcement.

5. The corrugated grout tube connections were shown to be effective splice connections for precast walls. A minimum average bond stress of 2.2 MPa was observed, which corresponds to a bond stress of approximately $0.4\sqrt{f_{cm}}$. The maximum bond stress of the corrugated grout tubes would likely be significantly higher than this, however this does provide a good indication of the minimum bond stress of the grout tubes.
6. The corrugated grout tube prevents local bar buckling of the dowel bar when the cyclic inelastic behaviour is concentrated at the base of these connections.
7. Walls detailed with a single central layer of vertical and horizontal reinforcement perform significantly worse under reversed cyclic loading than walls that are reinforced with a layer of vertical and horizontal reinforcement on each face. It was shown experimentally that they undergo significantly higher amounts of out-of-plane displacement and bar buckling behaviour is initiated after much smaller tension strain values.
8. Low ductility reinforcement (i.e. D500L mesh) extremely inhibits an elements ability to develop distributed cracking with distributed plasticity due to the limited amount of strain hardening the bar is able to undergo. It was shown experimentally that the low strain hardening ratio of the bars result in all the plastic deformations being concentrated in one crack, which then coupled with the low ultimate strain of the bars, leads to bar fracture at a much smaller displacement increment.

ACKNOWLEDGMENTS

The authors would like to thank the Brown family for their generous donation in establishing the Dr. William Piper Brown AM Scholarship, of which the lead author was the recipient. Financial support from the Australian Research Council (ARC) Discovery Project

DP140103350 entitled *Collapse Assessment of Reinforced Concrete Buildings in Regions of Lower Seismicity* is gratefully acknowledged.

REFERENCES

1. Wallace, J.W., 2012, "Performance of Structural Walls in Recent Earthquakes and Tests and Implications for US Building Codes", *Proceedings of the 15th World Conference on Earthquake Engineering*, Lisboa.

2. Elwood, K.J., 2013, "Performance of concrete buildings in the 22 February 2011 Christchurch earthquake and implications for Canadian codes", *Canadian Journal of Civil Engineering*, Vol. 40(3), pp. 759-776.

3. Sritharan, S., Beyer, K., Henry, R.S., Chai, Y.H. and Bull, M.K.D., 2014, "Understanding Poor Seismic Performance of Concrete Walls and Design Implications", *Earthquake Spectra*, Vol. 30(1), pp. 307-334.

4. Dashti, F., Dhakal, R.P. and Pampanin, S., 2017, "Tests on slender ductile structural walls designed according to New Zealand Standard", *Bulletin of the New Zealand Society for Earthquake Engineering*, Vol. 50(4), pp. 504-516.

5. Dashti, F., Dhakal, R.P. and Pampanin, S., 2017, "Numerical Modeling of Rectangular Reinforced Concrete Structural Walls", *Journal of Structural Engineering*, Vol. 143(6), Article number 04017031.

6. Rosso, A., Almeida, J.P. and Beyer, K., 2016, "Stability of thin reinforced concrete walls under cyclic loads: state-of-the-art and new experimental findings", *Bulletin of Earthquake Engineering*, Vol. 14(2), pp. 455-484.

7. Paulay, T. and Priestley, M.J.N., 1993, "Stability of Ductile Structural Walls", *ACI Structural Journal*, Vol. 90(4), pp. 385-392.

8. Segura, C.L. and Wallace, J.W., 2018, "Seismic Performance Limitations and Detailing of Slender Reinforced Concrete Walls", *ACI Structural Journal*, Vol. 115(3), pp. 849-859.

9. American Concrete Institute, 2014, *ACI 318-14 Building Code Requirements for Structural Concrete*, American Concrete Institute, Farmington Hills, MI.

10. Standards New Zealand, 2006, *NZS 3101:Part 1:2006 Concrete Structures Standard Part 1 - The Design of Concrete Structures*, Standards New Zealand, Wellington.

11. Standards Australia, 2009, *AS 3600-2009 Concrete structures*, SAI Global Limited, Sydney, NSW.

12. Menegon, S.J., Wilson, J.L., Lam, N.T.K. and Gad, E.F., 2017, "RC Walls in Australia: Reconnaissance Survey of Industry and Literature Review of Experimental Testing", *Australian Journal of Structural Engineering*, Vol. 18(1), pp. 24-40.

13. Patel, V.J., Van, B.C., Henry, R.S. and Clifton, G.C., 2015, "Effect of reinforcing steel bond on the cracking behaviour of lightly reinforced concrete members", *Construction and Building Materials*, Vol. 96, pp. 238-247.

14. Segura, C.I., Wallace, J.W., Arteta, C.A. and Moehle, J.P., 2016, "Deformation capacity of thin reinforced concrete shear walls", *Proceedings of the 2016 New Zealand Society of Earthquake Engineering Technical Conference*, Christchurch, New Zealand.

15. Taleb, R., Tani, M. and Kono, S., 2016, "Performance of Confined Boundary Regions of RC Walls Under Cyclic Reversal Loadings", *Journal of Advanced Concrete Technology*, Vol. 14, pp. 108-124.

16. Welt, T.S., Massone, L.M., Lafave, J.M., Lehman, D.E., Mccabe, S.L. and Polanco, P., 2017, "Confinement Behavior of Rectangular Reinforced Concrete Prisms Simulating Wall Boundary Elements", *Journal of Structural Engineering*, Vol. 143(4), Article number 04016204.

17. Hilson, C.W., 2014, *Analytical and Experimental Studies of the Seismic Performance of Reinforced Concrete Structural Wall Boundary Elements*, Doctor of Philosophy thesis, Civil Engineering, University of California, Los Angeles.

18. Rosso, A., Jimenez-Roa, L.A., Almeida, J.P., Zuniga, A.P.G., Blandon, C.A., Bonett, R.L. and Beyer, K., 2018, "Cyclic tensile-compressive tests on thin concrete boundary elements with a single layer of reinforcement prone to out-of-plane instability", *Bulletin of Earthquake Engineering*, Vol. 16(2), pp. 859-887.

19. Standards Australia and Standards New Zealand, 2001, *AS/NZS 4671:2001 Steel reinforcing materials*, Standards Australia International Ltd and Standards New Zealand, Sydney and Wellington.

20. Menegon, S.J., 2018, *Displacement Behaviour of Reinforced Concrete Walls in Regions of Lower Seismicity*, Doctor of Philosophy thesis, Department of Civil and Construction Engineering, Swinburne University of Technology.

21. Seifi, P., Henry, R.S. and Ingham, J.M., 2016, "Panel Connection Details in Existing New Zealand Precast Concrete Buildings", *Bulletin of the New Zealand Society for Earthquake Engineering*, Vol. 49(2), pp. 190-199.

22. Scott, B.D., Park, R. and Priestley, M.J.N., 1982, "Stress-strain Behavior of Concrete Confined by Overalapping Hoops at Low and High Strain Rates", *ACI Structural Journal*, Vol. 79(1), pp. 13-27.

23. Paulay, T. and Priestley, M., 1992, *Seismic Design of Reinforced Concrete and Masonry Buildings*, Wiley, New York.

24. Lu, Y., Henry, R.S., Gultom, R. and Ma, Q.T., 2017, "Cyclic Testing of Reinforced Concrete Walls with Distributed Minimum Vertical Reinforcement", *Journal of Structural Engineering*, Vol. 143(5), Article number 04016225.

25. Lu, Y. and Henry, R.S., 2017, "Numerical modelling of reinforced concrete walls with minimum vertical reinforcement", *Engineering Structures*, Vol. 143, pp. 330-345.

26. Hoult, R., Goldsworthy, H. and Lumantarna, E., 2018, "Plastic Hinge Length for Lightly Reinforced Rectangular Concrete Walls", *Journal of Earthquake Engineering*, Vol. 22(8), pp. 1447-1478.

27. Menegon, S.J., Wilson, J.L., Lam, N.T.K. and Gad, E.F., 2017, "Comprehensive Experimental Testing Program of Limited Ductile Reinforced Concrete Walls", *Proceedings of the Australian Earthquake Engineering Society 2017 Conference, November 24-26*, Canberra, ACT.

28. Menegon, S.J., Wilson, J.L., Lam, N.T.K. and Mcbean, P., 2018, "RC Walls in Australia: Seismic Design and Detailing to AS 1170.4 and AS 3600", *Australian Journal of Structural Engineering*, Vol. 19(1), pp. 67-84.

29. Chai, Y.H. and Elayer, D.T., 1999, "Lateral Stability of Reinforced Concrete Columns under Axial Reversed Cyclic Tension and Compression", *ACI Structural Journal*, Vol. 96(5), pp. 780-789.

TABLES AND FIGURES

List of Tables:

List of Figures:

Table 1 – Test specimen properties

	Specimen	H_w (mm)	t_w (mm)	H_w/t_w	Reinf. layout	Vertical reinf.	Reinf. ratio	Splice detail
Type 1	P01	2000	130	15.4	each face	6-N12	0.012	none
	P02	2000	130	15.4	each face	6-N12	0.012	none
	P03	2000	130	15.4	each face	6-N16	0.021	none
	P04	2000	130	15.4	each face	6-N16	0.021	none
	P05	2000	130	15.4	central	3-N12	0.006	none
	P06	2000	130	15.4	Central	3-N12	0.006	none
Type 2	P07	800	130	6.2	each face	6-N10	0.008	none
	P08	800	130	6.2	each face	6-N16	0.021	none
	P09	800	130	6.2	central	3-N10	0.004	none
	P10	800	130	6.2	central	3-N16	0.010	none
	P11	800	150	2.7*	each face	6-N10	0.007	lap splice
	P12	800	150	2.7*	each face	6-N12	0.010	lap splice
	P13	850	150	2.8*	each face	4-N10	0.005	lap splice
	P14	850	150	2.8*	each face	6-N16	0.018	lap splice
	P15	850	150	2.8*	each face	8-N12	0.013	precast
	P16	850	150	2.8*	each face	6-N12	0.010	precast
	P17	850	150	2.8*	each face	6-L11.9	0.010	precast

* Test specimens P11 to P17 were tested with a mid-height out-of-plane roller support to prevent out-of-plane buckling, which meant the slenderness ratio of the wall equal to $0.5 \times (H_w/t_w)$.

Table 2 – Loading protocol summary

Specimen	**Loading protocol**
P01 and P05	Quasi-static monotonic axial compression loading
P04	Quasi-dynamic cyclic axial tension-compression loading
P02, P03 and P06 to P17	Quasi-static cyclic axial tension-compression loading

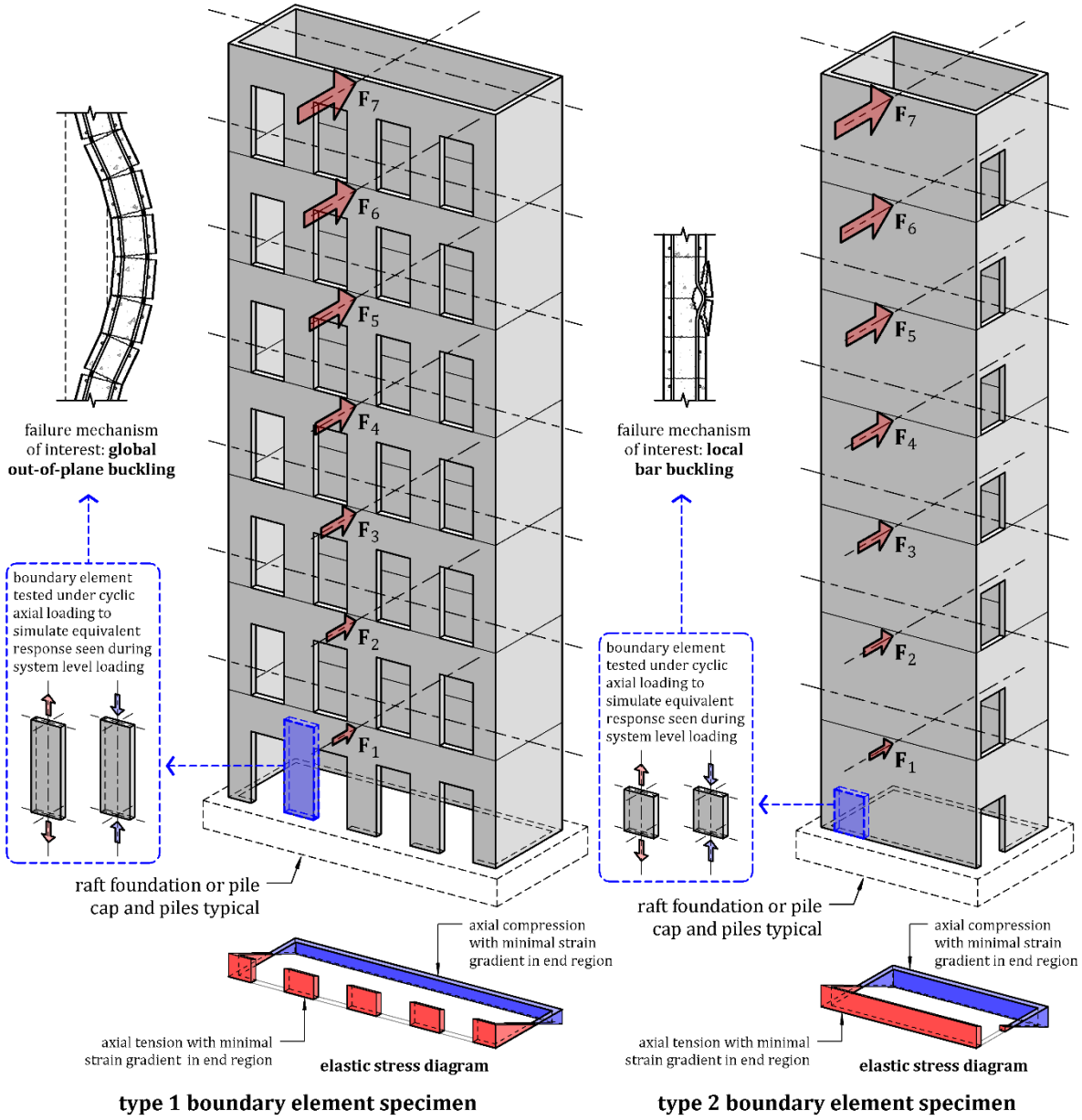

Fig. 1 – Proposed failure mechanisms for type 1 and type 2 specimens.

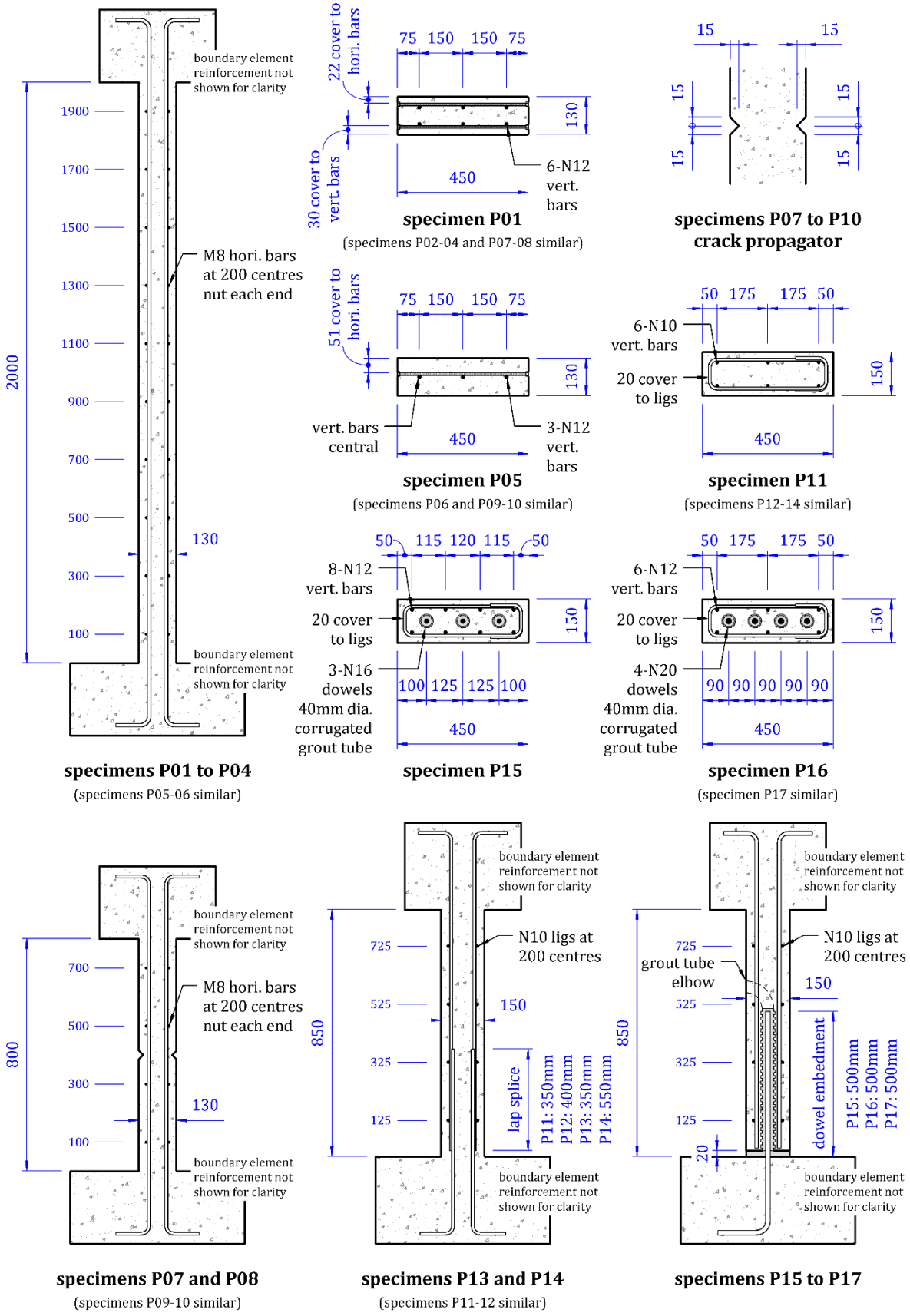

Fig. 2 – Test specimen overview.

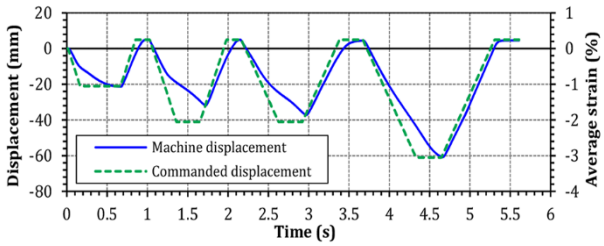

Fig. 3 – Test specimen P04 quasi-dynamic loading protocol.

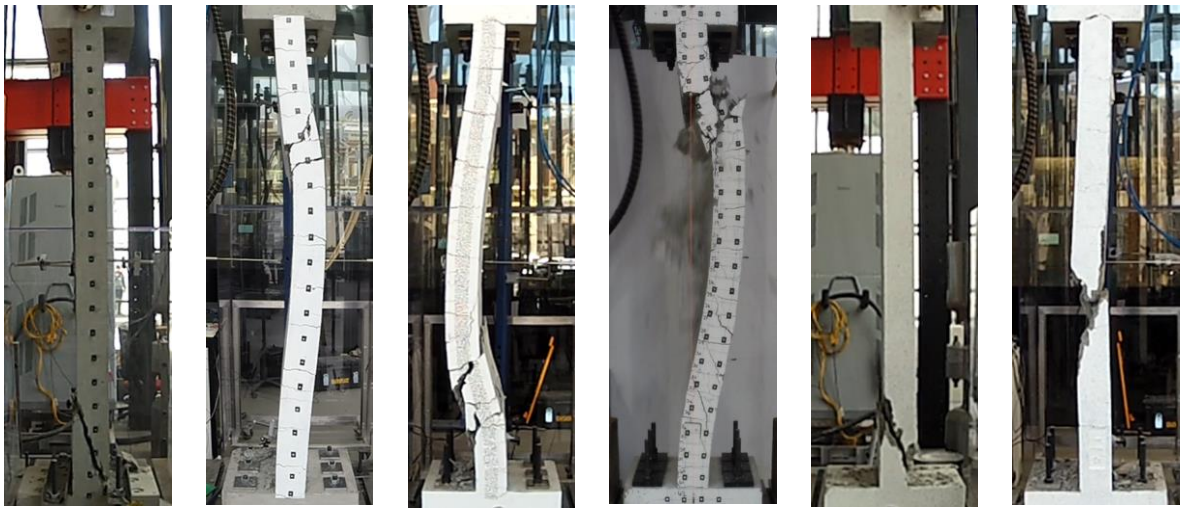

(a) P01 **(b) P02** **(c) P03** **(d) P04** **(e) P05** **(f) P06**

Fig. 4 – Failure photos of the type 1 boundary element specimens (P01 to P06).

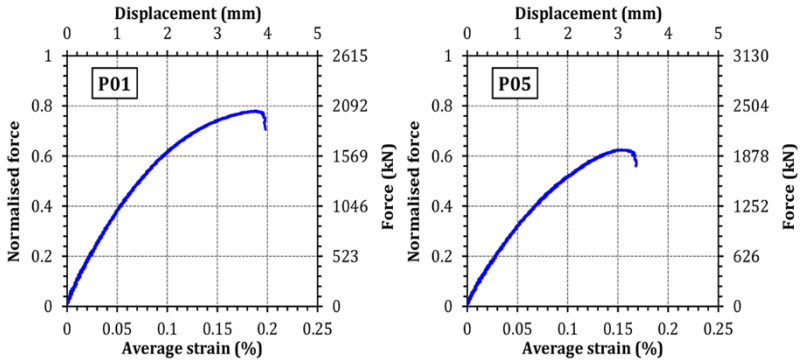

Fig. 5 – Force-displacement response of specimens P01 and P05.

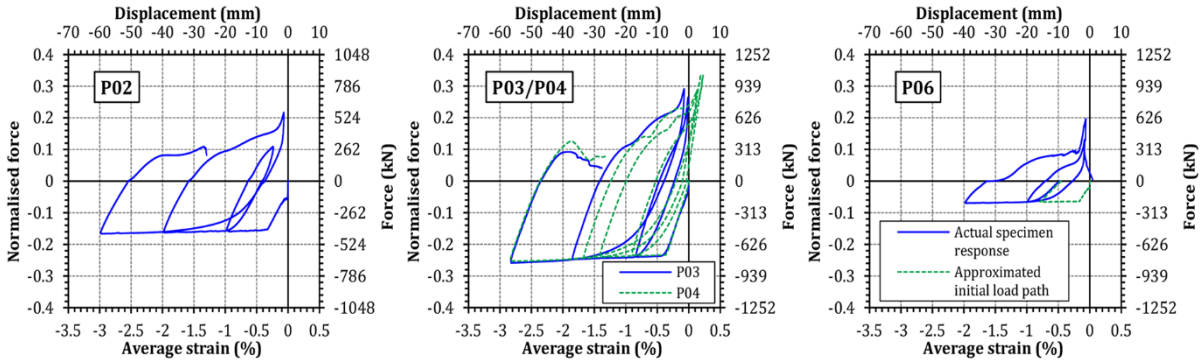

Fig. 6 – Force-displacement response of specimens P02 to P04 and P06.

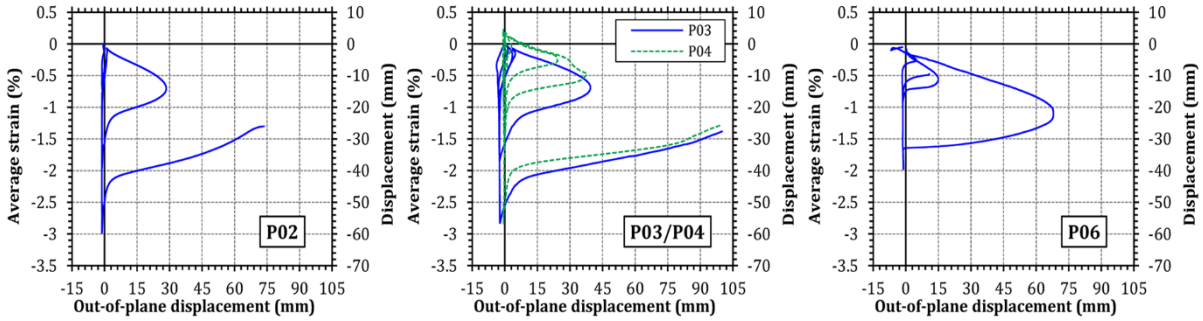

Fig. 7 – Out-of-plane displacement behaviour of specimens P02 to P04 and P06.

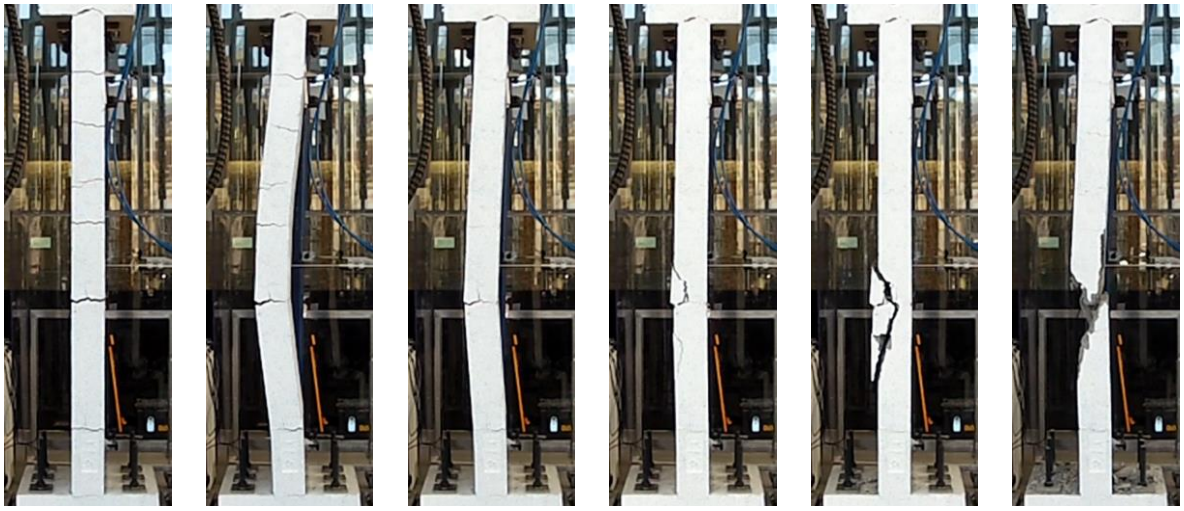

(a) tension displacement | **(b) buckling initiated** | **(c) buckling self-corrected** | **(d) crack closure** | **(e) local bar buckling** | **(f) loss of strength**

Fig. 8 – Failure progression of specimen P06 in load cycle 2.

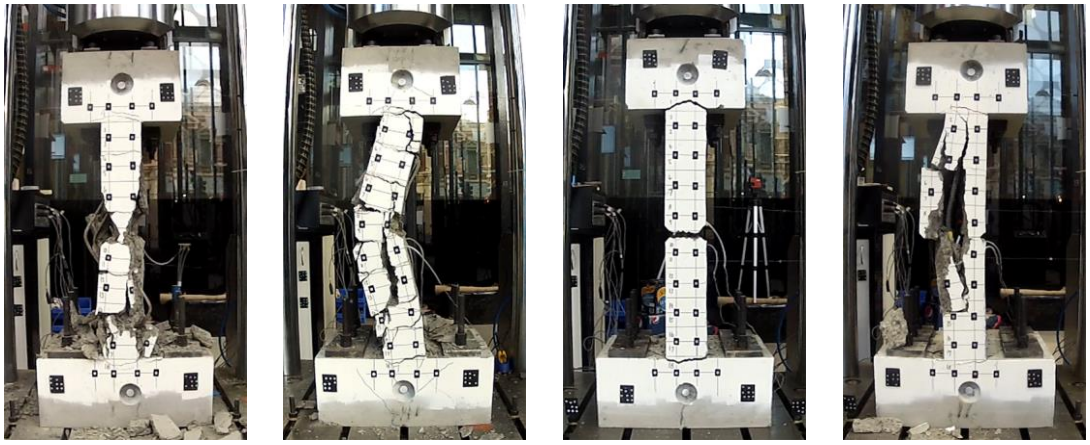

(a) P07 **(b) P08** **(c) P09** **(d) P10**

Fig. 9 – Failure photos of the type 2 boundary element specimens (P07 to P10).

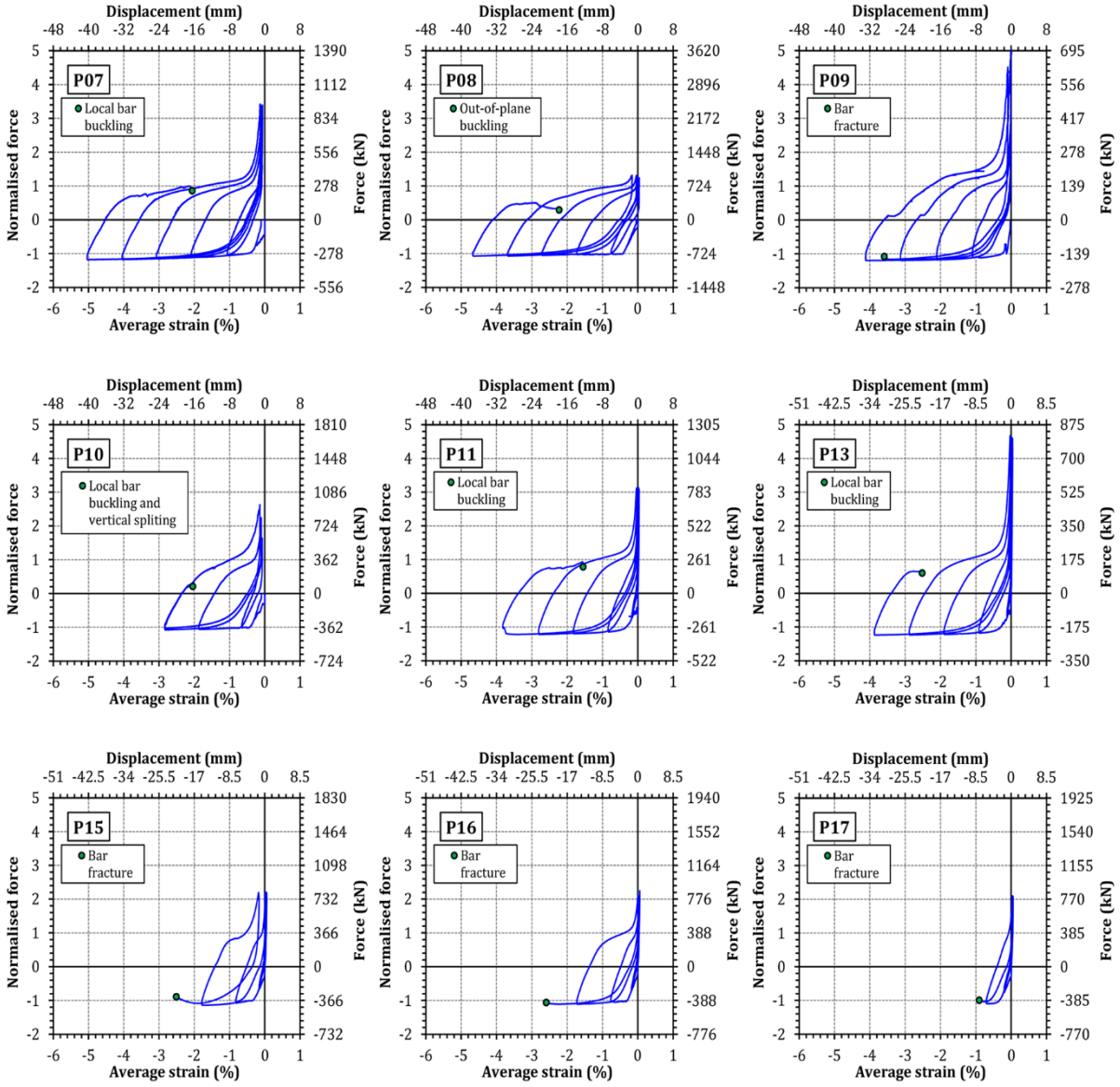

Fig. 10 – Force-displacement response of specimens P07 to P11, P13 and P15 to P17.

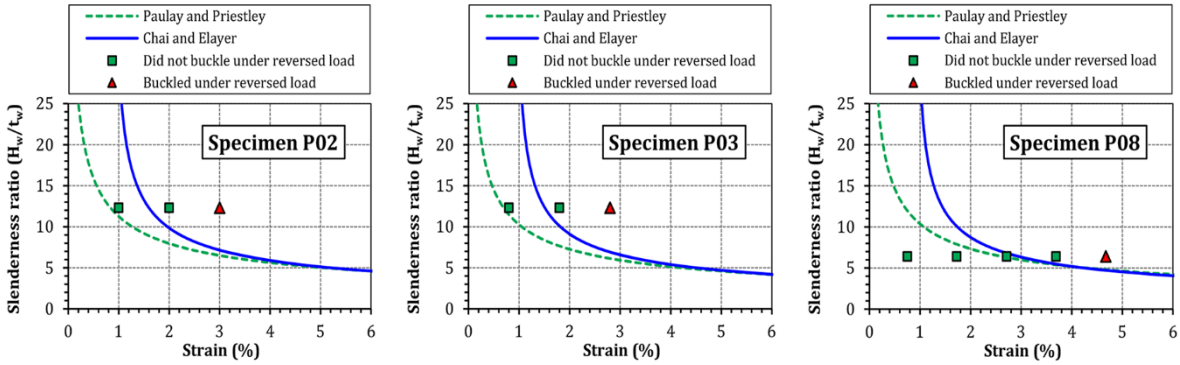

Fig. 11 – Comparison of out-of-plane buckling results and models in literature.